Effective Diffusivity by Pulse Gas Chromatography at Elevated Pressures

Pulse gas chromatography experiments at ambient pressure are often limited by an overwhelming contribution of axial dispersion to the observed variance and the inability to obtain a quantitative correction for this factor. Theoretically, the axial dispersion contribution can be reduced and at the same time the contribution due to particle diffusion can be enhanced by operating at elevated pressures. Our experiments on methane/helium diffusion in 0.32-cm-diameter commercial catalyst particles confirm this, and a new means of accounting for axial dispersion is demonstrated.

S. K. Sarmah
H. W. Haynes, Jr.
Chemical Engineering Department
University of Wyoming
Laramie, WY 82071

Introduction

Pulse gas chromatography has been widely applied to measurements of effective diffusivity in porous catalysts. The results obtained by this method, however, are not always reliable, and from a survey of the literature one might conclude that the method is limited to measurements on unusually large particles or to measurements on particles in which the mass transport rate is unusually slow. The factors responsible for this limited applicability are: 1. the overwhelming contribution of axial dispersion to the observed peak broadening or variance, which happens often; 2. the lack of a precise means of accounting for this axial dispersion contribution.

A case in point is the study by Sarma (1974; Sarma and Haynes, 1974) devoted to macropore diffusion in commercial catalyst particles. Here it was found that axial dispersion was responsible for typically 50 to 80% of the observed variance. Because the correction for axial dispersion was imprecise, it was not possible to obtain quantitative values of effective diffusivity.

Several methods have been employed to correct for axial dispersion. The earliest procedure employed a separate "blank" experiment on a bed of nonporous particles identical in size and shape to the catalyst particles. Since there can be no particle-associated transport resistances in this experiment, the sole contributor to peak broadening is axial dispersion. While some success has been achieved with this method, the practicality of dumping and repacking a column in a reproducible fashion has been questioned (Roemer et al., 1962; Gunn, 1968). Also, it has been shown that intraparticle diffusion may contribute to axial dispersion at low velocities (Wakao, 1976), so the blank experiment may underestimate the extent of axial dispersion in this region. Another common procedure is to assume a form for the velocity dependence of the axial dispersion coefficient and to then regress on velocity-dependent data. Unfortunately the nature of this velocity dependence varies greatly from column to column (Hsiang and Haynes, 1977), and the unwary investigator is apt to confound the eddy diffusion contribution to peak broadening with the particle diffusion contribution. In yet another procedure, Haynes and coworkers (Hsu and Haynes, 1981; Fu et al., 1986) calculated axial dispersion coefficients in columns of pilled and crushed large-pore zeolites from experiments with small-diameter permanent gases. Since these components diffuse rapidly, the only contribution to peak broadening is axial dispersion. A dimensionless correlation was developed for the axial dispersion coefficient. A similar approach was employed by Ruthven and coworkers (Ruthven and Kumar, 1979; Kumar et al., 1982) while investigating diffusion in small-pore zeolites. They calculated axial dispersion coefficients from experiments with large diameter molecules which could not penetrate the zeolite crystals. The advantage of this procedure is that the axial dispersion measurement is conducted on the identical bed to be subjected to the particle diffusivity experiment. However, it is not generally applicable.

The axial dispersion problem has thus plagued practitioners of pulse chromatography since the original work appeared in the mid 1960's. Despite innovative attempts to circumvent the problem there still is no generally applicable means available. In the present contribution we describe and demonstrate a procedure which not only enhances the particle diffusion terms relative to axial dispersion, but it also provides an automatic quantification of axial dispersion in the sample column.

Theory

The essence of our method is best understood from an inspection of the moments equations for the unit impulse response curve (Haynes and Sarma, 1973; Hashimoto and Smith, 1973;

Ma and Mancel, 1973):

$$\mu = \frac{L}{v}\left[\epsilon_z + (1-\epsilon_z)\epsilon_a + (1-\epsilon_z)(1-\epsilon_a)\epsilon_i(1+K)\right] \quad (1)$$

$$\sigma^2 = \frac{2LD_z}{v^3}\left[\epsilon_z + (1-\epsilon_z)\epsilon_a + (1-\epsilon_z)(1-\epsilon_a)\epsilon_i(1+K)\right]^2 + \frac{2L(1-\epsilon_z)[\epsilon_a + (1-\epsilon_a)\epsilon_i(1+K)]^2 R_a}{3vk_c} + \frac{2L(1-\epsilon_z)[\epsilon_a + (1-\epsilon_a)\epsilon_i(1+K)]^2 R_a^2}{15vD_a^e} + \frac{2L(1-\epsilon_z)(1-\epsilon_a)\epsilon_i^2(1+K)^2 R_i^2}{15vD_i^e} \quad (2)$$

Since these equations are well-known, an elaboration hardly seems necessary. Suffice it to say that the mean, μ, and variance, σ^2, are experimental quantities calculated from integrations on the finite pulse input and response curves. Only the Henry's law constant, K, appears in the first moment. The transport parameters appear in the variance or second moment about the mean. In our experiment the terms due to convective mass transport, k_c, and microparticle diffusion, D_i^e, are small and can be neglected. Only the axial dispersion term, D_z, and macropore diffusion term, D_a^e must be treated.

Critical to our analysis is the observation that the axial dispersion term appears in the numerator, whereas the particle mass transfer terms appear in the denominator of Eq. 2. In the regime where molecular diffusion contributes to mass transport, one can thus enhance the particle diffusion terms by operating at elevated pressures. (The molecular diffusivity is inversely proportional to pressure.) At the same time the axial dispersion term is reduced provided that velocities are so low that molecular diffusion has a role in the axial dispersion. Furthermore, the form of the pressure, temperature, and velocity dependence of the transport parameters is easily established. One can thus regress on a set of data consisting of pulse dispersion experiments at various temperatures, pressures, and velocities to obtain values of the transport coefficients.

The usual procedure of regressing on velocity alone can provide erroneous results. This is immediately apparent when Eq. 3 is substituted into Eq. 2.

$$D_z = \alpha D_M + \beta v^n \quad (3)$$

The first term in this equation accounts for the molecular diffusion contribution to axial dispersion, whereas the second term arises from mixing in the voids between particles or from nonuniform flow. Both α and β are explicitly dependent upon the column packing. Hsiang and Haynes (1977) found $1.3 < n < 1.9$ in beds of large spherical particles. The limit $n = 2$ corresponds to annular flow (Aris, 1959). Thus if flow down the wall is substantial, as commonly occurs, the βv^n or eddy diffusion term cannot be distinguished from the particle transport terms in Eq. 2. The investigator may report an effective diffusivity when in fact he is observing eddy diffusion in the voids between particles.

For a given column, α, β and n in Eq. 3 are constants. The pressure and temperature dependence of the molecular diffusivity can be ascertained from published data. This relation is usually of the form:

$$D_M = a\,T^b/P \quad (4)$$

and a and b can be evaluated for a particular gas pair. The Knudsen diffusivity is proportional to $\sqrt{T}$, or:

$$D_K = c\,T^{0.5} \quad (5)$$

and c is calculated from pore structure information and properties of the diffusant molecule. Generally the diffusant is highly diluted in the carrier gas, hence the Bosanquet equation for the transition diffusivity applies:

$$\frac{1}{D_T} = \frac{1}{D_K} + \frac{1}{D_M} \quad (6)$$

Finally, the effective diffusivity, D_a^e, is related to the transition diffusivity by an unknown geometric factor, g:

$$D_a^e = g\,D_T \quad (7)$$

The purpose of the experiment is to evaluate g.

The unknown parameters in Eqs. 3 to 7 are α, β, n and g. Substituting from these expressions into Eq. 2 provides:

$$\sigma_c^2 = \sigma_c^2(T, P, v, \alpha, \beta, n, g) \quad (8)$$

where the first three variables, i.e., T, P and v, are known independent variables. The column length, L, and the porosities, ϵ, are measured independently, and the Henry's law constant, K, is obtained from a regression on the first moment, Eq. 1. Thus the problem boils down to a nonlinear regression problem. We chose as our objective function the normalized sum of squares:

$$NSS = \sum\left[\frac{\sigma^2 - \sigma_c^2}{\sigma_c^2}\right] \quad (9)$$

A Taylor Series linearization procedure was employed to search for the minimum NSS.

Experimental Apparatus

A schematic of the apparatus is provided in Figure 1. Pure carrier gas flows continuously through a heated column packed with catalyst. A pulse of diffusing gas is injected into the inlet stream by means of an automatic air-activated sample valve. Splitting tees at both the inlet and outlet of the column divert a small amount of gas to flame ionization detectors where the methane concentration is monitored. The signal from the FID electrometers is amplified, passed to an automatic data acquisition system, and digital results are stored on floppy disks for later analysis. To aid in the operation of the system the electrometer signals are also monitored on a strip chart recorder. Pressure drop across the column is monitored continuously by a differential pressure cell. The apparatus can be operated at pressures from ambient to 1.72 MPa.

A special capillary arrangement was devised to allow the column to operate at elevated pressures while the detectors are at ambient pressure. This is illustrated in Figure 2. Two thermostated capillaries, one in the oven and one in the detector hous-

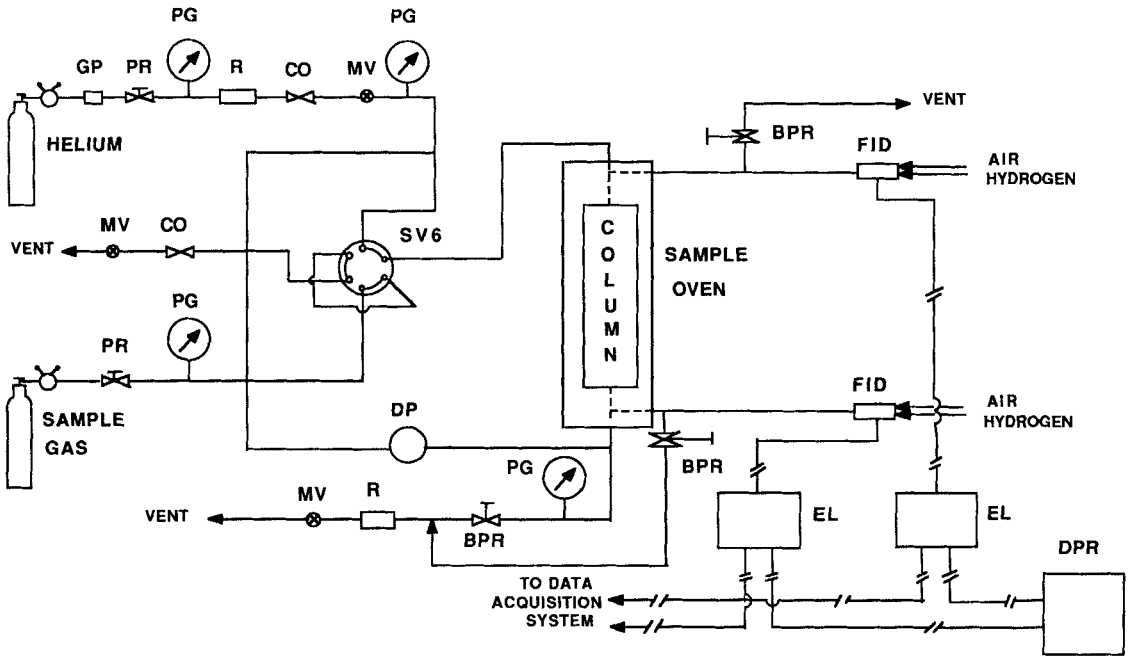

Figure 1. GC diffusivity apparatus.

ing, were sized to take most of the pressure drop between the column and detector. The oven capillary could be changed conveniently as pressure was varied. A third permanent capillary was installed between the supply line and detector. The flow rate to the detector could be controlled by varying the supply line pressure by means of a back-pressure regulator. A flow calibration curve was developed for both the inlet and outlet FID capillaries by monitoring the flow rate as a function of pressure. The inlet supply line was vented through a rotameter; however, the outlet supply line was returned to the column outlet stream. Thus the column flow rate could be accurately determined by monitoring the effluent rate and adding the small flow to the outlet detector obtained from the FID capillary calibration curve.

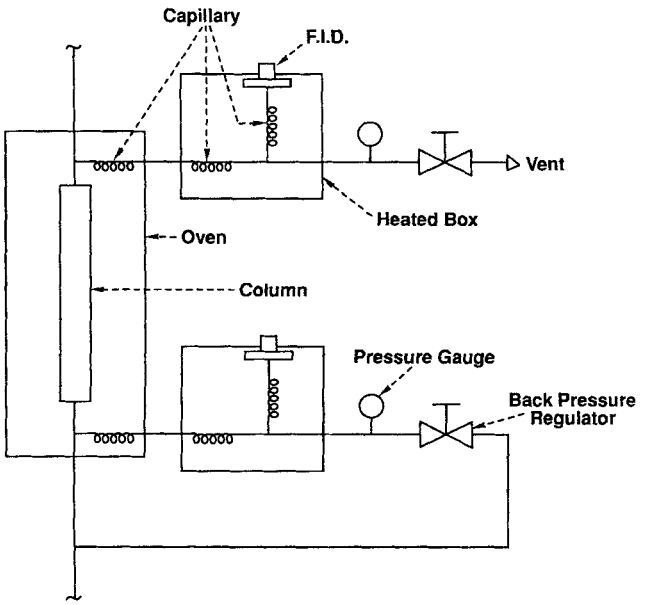

Figure 2. Detector capillary arrangement.

This arrangement effectively served to eliminate corrections for extra column dispersion. Due to high velocities in the capillary tubes, the extent of dispersion was small. This, coupled with the fact that identical inlet and outlet dispersions will cancel, made it unnecessary to correct the observed variance. A small correction was made to the observed mean to account for the fact that flows through the inlet and outlet detector supply lines differed slightly.

The catalyst chosen for this study was a commercial CoMo/Alumina catalyst manufactured by Harshaw and identified as CoMo-0601. It is in the form of well-defined 0.32-cm-dia. × 0.32-cm-long cylindrical tablets. Pore-size distribution determinations by both mercury porosimetry and nitrogen adsorption revealed a bimodal pore structure, Figure 3. Only pores larger than approximately 6 nm could be accessed by our mercury porosimeter (assuming a contact angle at 130°). The pore-size distribution in pores smaller than 10 nm was calculated from the desorption branch of the isotherm using the BJH algorithm (Barrett et al., 1951) with the nonclassical Kelvin equation as recommended by Broekhoff and deBoer (1968). The average macropore and micropore radii are compiled with other physical properties in Table 1.

Methane was chosen as the diffusant because of its low molecular weight (high diffusivity). The carrier gas was helium.

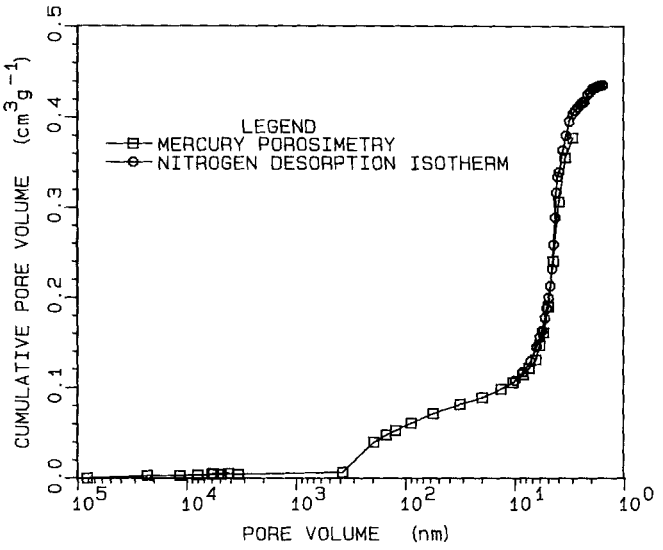

Figure 3. Cumulative pore-size distribution, Harshaw CoMo-0601.

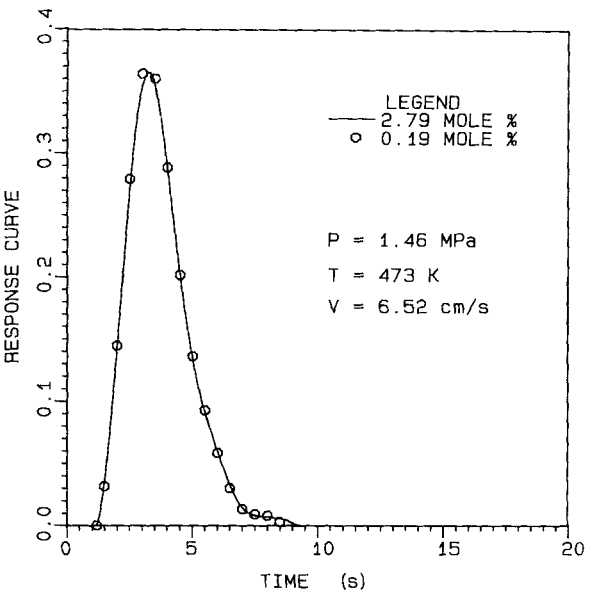

Figure 4. Effect of pulse concentration on response curves.

Past experience had indicated that rapid diffusion in such small catalyst particles would be difficult or impossible to detect by pulse chromatography at ambient pressure. Thus the system selected for study is a rather severe test of our ability to evaluate effective diffusivities by the proposed new method.

Most of the experimentation was conducted in a 61.0-cm-long column of 1.09-cm inside diameter. The bed porosity, calculated from the measured bulk density and apparent particle density, was 0.36. To remove adsorbed moisture from the catalyst particles, the column was heated to 200°C for 24 hours under flowing helium prior to conducting a series of experiments.

Results

Linearity testing

Equations 1 and 2 were derived from a linear chromatography theory. In particular the adsorption isotherm is assumed to be in the Henry's law region and the diffusion is assumed to be Fickian. Either of these assumptions might be in jeopardy if the diffusant concentration becomes too high. Accordingly, a series of linearity tests was conducted to insure that the column is indeed operating in the linear region. The demonstration of system linearity also insures that no adsorption heat effect is present provided that the column operates at infinite dilution (Haynes, 1986).

Dilute mixtures of methane in helium were prepared and analyzed by gas chromatography. A series of pulse dispersion tests was conducted in which high and low concentrations of methane were injected via the sample injection valve while column conditions remained constant. The response curves from a pair of experiments are plotted in Figure 4. The coincidence of these curves in view of the over tenfold difference in concentrations is proof of system linearity. All subsequent injections were within this concentration range.

Table 1. Properties of Catalyst Particles

Size	0.32 cm dia. × 0.32 cm long
Apparent Density	1.39 g/cm³
BET Surface Areas	130 m²/g
Pore Volume	0.43 cm³/g
Macropore Porosity	0.11
Avg. Macropore Radius	209 nm
Micropore Porosity	0.55
Avg. Micropore Radius	5.5 nm

Static measurements of K

As shall be demonstrated in the next section, evaluation of the Henry's law constant is readily accomplished by pulse chromatography from an analysis of the first moment using Eq. 1. For comparison purposes, an independent measurement was conducted in a static volumetric apparatus (Micromeritics Accusorb 2100E). Because methane is not strongly adsorbed at the elevated temperatures of this investigation, a large sample (≅15 g) was charged to the sample holder. Not only did this provide sufficient sensitivity for the determination, but it insured that the results of this test are representative of the entire catalyst lot.

Results from the static adsorption measurements at three different temperatures are plotted in Figure 5. From slopes of the straight line portion of these curves near the origin, the dimensionless Henry's law constants were evaluated using:

$$K = \frac{\rho_p T V_{STP}}{273.2\, \epsilon_i (1 - \epsilon_a) P} \tag{10}$$

A van't Hoff plot of these values was linear, and the heat of adsorption was calculated to be −11.7 kJ/mol. Values of K obtained from this plot are presented in Table 2 under the "static" heading.

First moment analysis

The results from 39 pulse testing experiments are compiled in Table 3. Pressure, temperature, and velocity have been varied over a wide range. The mean and variance were obtained from

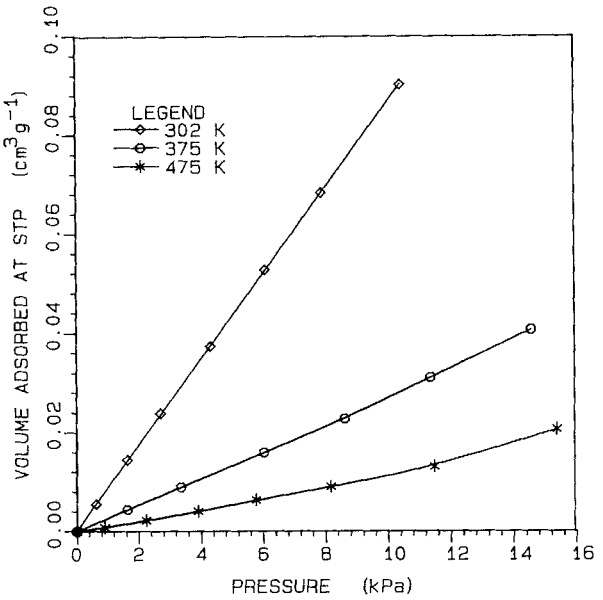

Figure 5. Methane adsorption isotherms by the static method.

integrations on the normalized input, $X(t)$, and output, $Y(t)$, pulses according to:

$$\mu_X = \int_0^\infty t\, X(t)\, dt \tag{11}$$

$$\mu_Y = \int_0^\infty t\, Y(t)\, dt \tag{12}$$

$$\mu = \mu_Y - \mu_X \tag{13}$$

$$\sigma_X^2 = \int_0^\infty (t - \mu_X)^2\, X(t)\, dt \tag{14}$$

$$\sigma_Y^2 = \int_0^\infty (t - \mu_Y)^2\, Y(t)\, dt \tag{15}$$

$$\sigma^2 = \sigma_Y^2 - \sigma_X^2 \tag{16}$$

As mentioned earlier, a small correction of the order of fractions of a second was made to the first moment to account for slight differences in the inlet and outlet detector flowrates.

According to Eq. 1, a plot of μ vs. $1/v$ at constant temperature should be a straight line through the origin. Such a plot is constructed in Figure 6, and agreement with the theory is excellent. Note that each curve is composed of points collected at different pressures. This provides further confirmation that Henry's law is valid at all pressures studied. Values of K were obtained from

Table 2. Henry's Law Constants: Static vs. Pulse Chromatography Experiments

Temp. K	Dimensionless Henry's Law Constant	
	Static	Chromatographic
303	2.65	2.73
373	1.12	1.32
473	0.51	0.64

Table 3. Pulse Testing Results

Pres. P MPa	Temp. T K	Vel. v cm/s	Exp. μ s	exp. σ^2 s^2	Contrib. of D_z to σ_c^2 %	Contrib. of D_a^e to σ_c^2 %
0.424	303	5.98	16.13	13.73	48.12	51.88
0.424	303	8.92	10.81	8.73	45.53	54.47
0.424	303	13.66	7.17	5.54	43.04	56.96
0.424	373	6.09	11.23	4.44	61.58	38.42
0.424	373	11.18	6.23	2.28	57.66	42.34
0.424	373	13.77	5.09	1.82	56.44	43.56
0.424	473	7.65	7.21	1.73	72.52	27.48
0.424	473	10.93	4.90	1.11	70.49	29.51
0.768	303	5.98	16.30	17.09	35.16	64.84
0.768	303	7.04	13.42	8.40	34.25	65.75
0.768	303	8.64	11.10	10.42	33.17	66.83
0.768	373	5.41	12.82	6.05	49.45	50.55
0.768	373	7.21	9.76	4.23	47.57	52.43
0.768	373	9.34	7.60	3.36	46.01	53.99
0.768	473	5.70	10.28	3.16	63.42	36.58
0.768	473	8.06	7.36	2.17	61.18	38.83
0.768	473	9.64	6.12	1.59	60.10	39.90
1.113	303	6.37	14.95	19.66	27.40	72.60
1.113	303	8.05	11.72	16.03	26.33	73.67
1.113	303	9.79	9.53	11.50	25.49	74.51
1.113	373	6.27	10.78	6.46	40.06	59.94
1.113	373	8.59	7.65	4.37	38.26	61.74
1.113	373	11.30	5.83	3.26	36.79	63.21
1.113	373	11.41	5.50	3.06	36.74	63.26
1.113	473	2.18	26.32	12.05	63.50	36.50
1.113	473	2.20	26.16	10.57	63.43	36.57
1.113	473	5.93	9.78	3.20	55.03	44.97
1.113	473	5.99	9.25	3.83	54.97	45.03
1.113	473	8.26	6.67	2.42	52.94	47.06
1.113	473	8.28	6.64	2.43	52.93	47.07
1.457	303	4.85	20.19	25.35	23.74	76.26
1.457	303	6.67	14.65	19.48	22.42	77.58
1.457	303	8.32	12.08	16.01	21.56	78.44
1.457	373	3.87	18.15	13.41	36.94	63.06
1.457	373	6.80	10.50	6.15	33.70	66.30
1.457	373	9.39	7.72	4.34	32.07	67.93
1.457	473	5.40	10.70	3.97	49.38	50.62
1.457	473	7.99	7.27	2.79	46.95	53.05
1.457	473	10.63	5.43	1.81	45.31	54.69

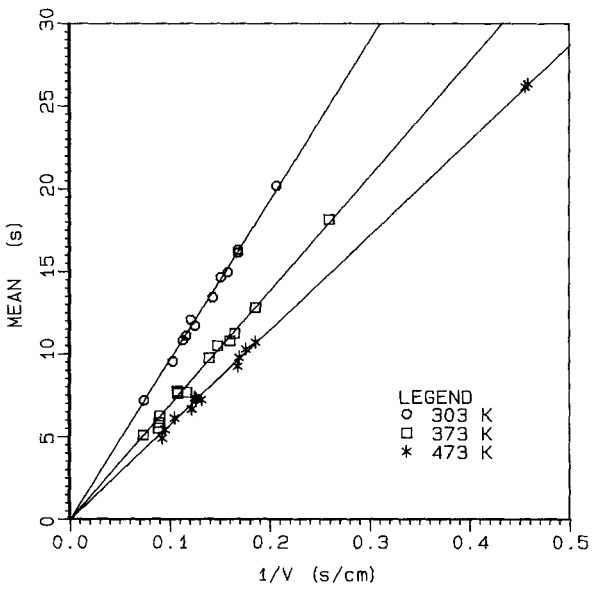

Figure 6. First moment plot.

the slopes of these curves and the known column and catalyst properties, Table 1. These constants are recorded in Table 2 for comparison with the values of K obtained from the static experiment. Agreement between the two is quite good although the static values tend to lie somewhat below the chromatographic values, especially at the higher temperatures.

Tests on a 30-cm column were also conducted, and the results may be found in Sarmah's thesis (Sarmah, 1988). Large discrepancies were observed between the chromatographic and static K values, and the shorter column results are thus believed to be unreliable. The discrepancy was evidently due to an end effect.

Second moment analysis

The constants, a and b, of Eq. 4 were evaluated from the methane-helium diffusivity data of Hu and Kobayashi (1970). The Knudsen diffusivity parameter c of Eq. 5 was calculated for methane diffusion in the macropores using the average macropore radius, Table 1.

Nonlinear regression on the data of Table 3 provided the following results:

$$D_z = 0.79\, D_M + 0.14\, v^{1.79} \tag{17}$$

and

$$D_a^e = 0.10\, D_T \tag{18}$$

Agreement between the calculated and experimental variances is good as indicated in the parity plot of Figure 7. However, agreement between variances is not sufficient proof that the model fits the data, since quite different response curves can produce identical first and second moments. Accordingly, several impulse response curves were deconvoluted from the $X(t)$ and $Y(t)$ using Fourier transforms with integrations by Filon's method. Time domain solutions to the model equations were similarly calculated from the inverse Fourier transform. The

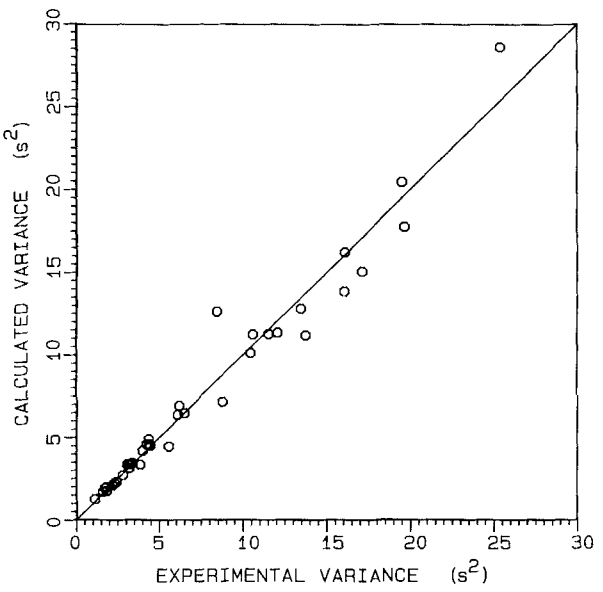

Figure 7. Parity plot for experimental and calculated variances.

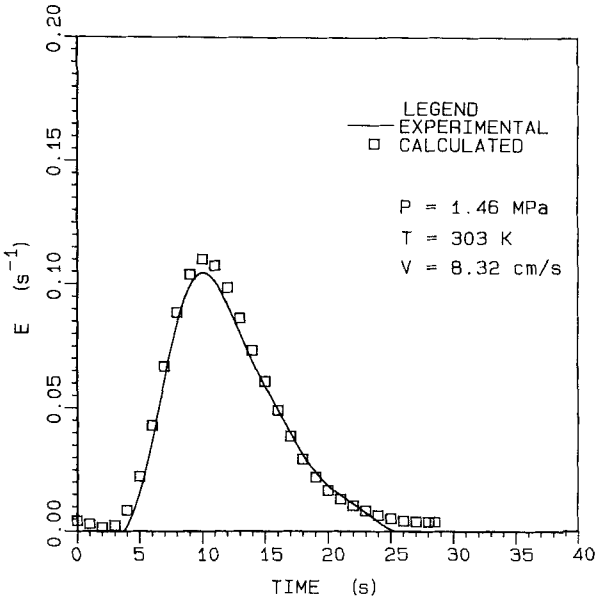

Figure 8. Impulse response curves: experimental vs. calculated.

results of a typical comparison are plotted in Figure 8. Agreement is very good, thus substantiating the ability of the model to describe these data.

Discussion

The parameter values obtained from the second moment analysis all appear quite reasonable. The factor $\alpha = 0.79$ in the molecular diffusion contribution to D_z, Eq. 17, corresponds to a bed tortuosity of 2.2. The exponent on velocity, $n = 1.79$, in this same expression is within the range observed by Hsiang and Haynes (1977) in pulse dispersion tests on nonporous particles. This value suggests that flow down the tube wall may be substantial. The geometric factor, $g = 0.10$, of Eq. 18 corresponds to a tortuosity factor of 1.1 using the macroporosity of 0.11, Table 1. Calculations on the parallel pore model indicate that diffusion through the micropores is comparable in magnitude to macropore diffusion. This could explain the somewhat low value of tortuosity.

The central idea behind this investigation is that the sensitivity to particle mass transport may be improved by operating at elevated pressures. It is interesting therefore to compare the axial dispersion and macropore diffusion contributions to variance. These contributions, expressed as a percentage, are also compiled in Table 3. As expected, the relative contribution due to macropore diffusion is enhanced at the higher pressures. Further calculations indicate that axial dispersion would account for 70 to 95% of the variance, had the experiment been conducted at atmospheric pressure. The effect of temperature is also significant. At a given pressure the particle diffusion contribution is greatest at the lowest temperatures. There is some enhancement of the macropore diffusion contribution at higher velocities, but this is not very pronounced.

Estimates of the convective mass transport and micropore diffusion contributions to variance were obtained by calculating the respective terms in Eq. 1. The convective mass transport coefficient, k_c, was estimated from the correlation of Wakao and

Funazkri (1978). The microparticle effective diffusivity, D_i^e, was estimated from the Wheeler (1955) model using a tortuosity factor of three. The microparticle radius was assumed to be 50 μm. These calculations indicated that convective mass transport and micropore diffusion could account for only a small (negligible) percentage of the observed variance.

Conclusions

These test results have demonstrated that pulse gas chromatography can be used to evaluate effective diffusivities in porous catalysts of the size and type employed in commercial operations. By conducting the experiment at elevated pressure, the particle diffusion contribution to peak broadening is enhanced relative to the axial dispersion contribution. A regression on the data set, in which pressure, temperature, and velocity were varied, provided axial dispersion parameters simultaneously with the effective diffusivity.

Notation

a = parameter defined by Eq. 4
b = parameter defined by Eq. 4
c = parameter defined by Eq. 5
D^e = effective diffusivity, cm^2/s
D_K = Knudsen diffusivity, cm^2/s
D_M = molecular diffusivity, cm^2/s
D_T = transition region diffusivity, cm^2/s
D_z = axial dispersion coefficient, cm^2/s
g = geometric factor defined by Eq. 7
K = dimensionless Henry's law constant
k_c = convective mass transfer coefficient, cm/s
L = column length, cm
n = exponent on velocity, Eq. 3
P = pressure, MPa
R = particle radius, cm
T = temperature, K
t = time, s
V_{STP} = volume adsorbed at STP, cm^3/g
v = superficial velocity, cm/s
X = normalized input curve, s^{-1}
Y = normalized response curve, s^{-1}

Greek letters

α = parameter defined by Eq. 3
β = parameter defined by Eq. 3
ϵ = porosity
μ = mean, s
ρ_p = particle density, g/cm^3
σ^2 = variance, s^2

Subscripts

a = macropore quantity
c = calculated
i = micropore or microparticle quantity
X = input curve
Y = output curve
z = bed quantity

Literature Cited

Aris, R., "On the Dispersion of a Solute by Diffusion, Convection and Exchange Between Phases," *Proc. Roy. Soc.*, **A252,** 538 (1959).

Barrett, E. P., L. G. Joyner, and P. P. Halenda, "The Determination of Pore Volume and Area Distributions in Porous Substances. I. Computations from Nitrogen Isotherms," *J. Amer. Chem. Soc.*, **73,** 373 (1951).

Broekhoff, J. C. P., and J. H. deBoer, "Studies on Pore Systems in Catalysts XIII. Pore Distributions from the Desorption Branch of a Nitrogen Sorption Isotherm in the Case of Cylindrical Pores: B. Applications," *J. Cat.* **10,** 377 (1968).

Fu, C.-C., M. S. P. Ramesh, and H. W. Haynes, Jr., "Analysis of Gas Chromatography Pulse Dispersion Data for the System n-Butane/Zeolite NaY," *AIChE J.*, **32,** 1848 (1986).

Gunn, D. J., "Mixing in Packed and Fluidized Beds," *Chem. Engr.*, **219,** CE 153 (1968).

Hashimoto, N., and J. M. Smith, "Macropore Diffusion in Molecular Sieve Pellets by Chromatography," *Ind. Eng. Chem., Fund.*, **12,** 353 (1973).

Haynes, Jr., H. W., "An Analyses of Sorption Heat Effects in the Pulse Gas Chromatography Diffusion Experiment," *AIChE J.*, **32,** 1750 (1986).

Haynes, Jr., H. W., and P. N. Sarma, "A Model for the Application of Gas Chromatography to Measurement of Diffusion in Bidisperse Structured Catalysts," *AIChE J.*, **19,** 1043 (1973).

Hsiang, T. C.-S., and H. W. Haynes, Jr., "Axial Dispersion in Small Diameter Beds of Large, Spherical Particles," *Chem. Eng. Sci.*, **32,** 678 (1977).

Hsu, L.-K. P., and H. W. Haynes, Jr., "Effective Diffusivity by the Gas Chromatography Technique: Analysis and Application to Measurements of Diffusion of Various Hydrocarbons in Zeolite NaY," *AIChE J.*, **27,** 81 (1981).

Hu, A. T., and R. Kobayashi, "Measurements of Gaseous Diffusion Coefficients for Dilute and Moderately Dense Gases by Perturbation Chromatography," *J. Chem. Eng. Data*, **15,** 328 (1970).

Kumar, R., R. C. Duncan, and D. M. Ruthven, "A Chromatographic Study of Diffusion of Single Components and Binary Mixtures of Gases in 4A and 5A Zeolites," *Can. J. Chem. Eng.*, **60,** 493 (1982).

Ma, Y. H., and C. Mancel, "Diffusion of Hydrocarbons in Mordenites by Gas Chromatography," *Adv. Chem. Ser.*, **121,** 392 (1973).

Roemer, G., J. S. Dranoff and J. M. Smith, "Diffusion in Packed Beds at Low Flow Rates," *Ind. Eng. Chem., Fund.*, **1,** 284 (1962).

Ruthven, D. M., and R. Kumar, "A Chromatography Study of the Diffusion of N_2, CH_4 and Binary CH_4-N_2 Mixtures in 4A Molecular Sieve," *Can. J. Chem. Eng.*, **57,** 342 (1979).

Sarma, P. N., "Application of Gas Chromatography to Measurements of Diffusion in Bidisperse Structured Catalysts," PhD Diss., Univ. Mississippi, Oxford (1974).

Sarma, P. N., and H. W. Haynes, Jr., "Effective Macropore Diffusivity of Bidisperse Structured Catalysts by Gas Chromatography," AIChE Meeting, paper 65g, Washington, DC (1974).

Sarmah, S. K., "Effective Diffusivity by Pulse Gas Chromatography at Elevated Pressures," MS Thesis, Univ. of Wyoming, Laramie (1988).

Wakao, N., and T. Funazkri, "Effect of Fluid Dispersion Coefficients on Particle-to-Fluid Mass Transfer Coefficient in Packed Beds—Correlation of Sherwood Numbers," *Chem. Eng. Sci.*, **33,** 1375 (1978).

Wakao, N., "Particle-to-Fluid Transfer Coefficients and Fluid Diffusivities at Low Flow Rate in Packed Beds," *Chem. Eng. Sci.*, **31,** 1115 (1976).

Wheeler, A., "Reaction Rates and Selectivity in Catalyst Pores," *Adv. Cat.*, **III,** 249 (1951).

Manuscript received Mar. 28, 1989, and revision received Aug. 4, 1989.